

# Center Manifold Analysis of a Point–Vortex Model of Vortex Shedding with Control

Bartosz Protas

*Department of Mathematics & Statistics  
McMaster University, Hamilton ON Canada*

---

## Abstract

In this paper we use methods of dynamical systems theory to provide a precise mathematical characterization of the behavior of the point vortex Föppl system with linear feedback control. The Föppl system was used in an earlier investigation as a simple model for control design of vortex shedding and numerical studies indicated that the state of the controlled system converges to a closed orbit. In this investigation we prove rigorously that this observed behavior in fact represents periodic oscillations on the center manifold of the closed–loop nonlinear system. This manifold is shown to coincide with the uncontrollable subspace of the linearized system.

*Key words:* point vortices, flow control, dynamical systems, wake flows

*PACS:* 47.15.Hg, 47.27.Rc, 47.27.Vf

---

## 1 Introduction

Integration of rigorous methods of Modern Control Theory with Computational Fluid Dynamics has opened new possibilities in the field of Flow Control. This, in particular, concerns the design of feedback stabilization strategies based on Linear Control Theory which proved to be quite successful (see, e.g., the review papers [1,2]). Application of such methods, however, is limited by the need to solve a nonlinear operator Riccati equation required to determine the feedback operators. In practical applications such problems are usually computationally intractable, unless the underlying partial differential equation (PDE) describing evolution of perturbations has some special properties (e.g., decouples in Fourier space). Hence, in order to solve such problems in general settings one seeks simplified descriptions

---

*Email address:* [bprotas@mcmaster.ca](mailto:bprotas@mcmaster.ca) (Bartosz Protas).

*URL:* <http://math.mcmaster.ca/bprotas> (Bartosz Protas).

of the system, known as reduced-order models, that render the problem of determining feedback operators computationally tractable. One family of reduced-order models is based on point vortices which are weak (singular) solutions of the two-dimensional (2D) Euler equations. Point vortex systems have been used as a basis for design of flow control algorithms by several researchers, including Cortelezzi et al. [3–5], Chernyshenko [6], Péntek et al. [7], Noack et al. [9,10], Zannetti and Iollo [8], and Vainchtein and Mezić [11]. In particular, the Föppl system [12], representing a simple potential flow model for a 2D recirculating flow behind a circular cylinder, was employed to construct control strategies for the cylinder wake flow in the laminar regime in [13,14]. This model was subsequently used by the present author in [15] for a systematic design of a control strategy based on the linear control theory with the goal of stabilizing the equilibrium solution. The particular configuration considered in that investigation employed the cylinder rotation as the flow actuation (i.e., the control variable) and measurements of the velocity on the flow centerline downstream of the cylinder as the system output (Figure 1). Numerical simulations reported in [15] regarding application of such linear stabilization strategies to the Föppl system revealed an interesting behavior: the linear control algorithm was able to stabilize the otherwise exponentially unstable system, however, instead of asymptotic convergence to the equilibrium solution, the system trajectory would converge to a closed orbit encircling the equilibrium. Analogous results were also obtained applying this control strategy to stabilize an actual cylinder wake flow governed by the 2D Navier–Stokes equations at  $Re = 75$ . This is clearly an undesirable behavior, as it results in persistent oscillations in the closed-loop system. The purpose of this paper is to use methods of dynamical systems theory to provide a rigorous mathematical characterization of this observed behavior with the hope of using it to understand and improve the performance of vortex-based flow control strategies. The structure of the paper is as follows: in the next section we introduce formally the Föppl system and the associated control problem; we also briefly review the results obtained earlier with the linear stabilization algorithm, in the following Section we perform an invariant manifold reduction of the closed-loop system, in Section 4 we prove a theorem concerning stability of the reduced system on the center manifold and in Section 5 we present some numerical computations illustrating our findings; conclusions concerning relevance of these results to the observed behavior are deferred to Section 6. Many of the results presented in this paper required manipulation of rather complicated algebraic expressions, some of which are collected in Appendix A. Processing of such expressions was made possible by the use of a symbolic manipulation package MAPLE 10. The code which allows one to reproduce all the results presented in this paper is available at [http://www.math.mcmaster.ca/bprotas/Software/foppl\\_center\\_manifold](http://www.math.mcmaster.ca/bprotas/Software/foppl_center_manifold).

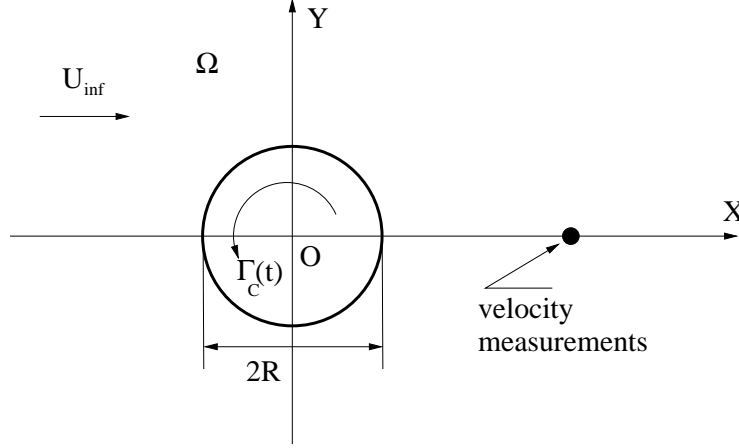


Fig. 1. Schematic of the wake stabilization problem.

## 2 Föppl System as Model for a Controlled Cylinder Wake Flow

In this Section we introduce the Föppl system and discuss briefly stability properties of its equilibrium solution. Then we formally state the control problem, characterize controllability of the linearized system, and review the stabilization strategy based on the linear control theory. Most of these results have been published elsewhere, hence our discussion here is concise and serves only to set the stage for subsequent developments.

We consider a 2D potential flow past a circular cylinder with radius  $R = 1$  in an unbounded domain such that velocity at infinity approaches a constant vector  $U_\infty \mathbf{e}_x$ , where for simplicity  $U_\infty = 1$  and  $\mathbf{e}_x$  is the unit vector of the X-axis. The Föppl system [12] is obtained by adding two counter-rotating point vortices with circulations  $-\Gamma$  and  $\Gamma$ , one above and one below the flow centerline, together with their images inside the obstacle, to the potential flow past the cylindrical obstacle (see Figure 2). The state of the system is characterized by positions of the two vortices  $z_1 = x_1 + iy_1$  and  $z_2 = x_2 + iy_2$ , where  $i = \sqrt{-1}$  (in our analysis below we will interchangeably use complex and real notation, as dictated by conciseness and clarity). Hence, the state evolution is governed by

$$\frac{d}{dt} \mathbf{X} = \mathbf{F}(\mathbf{X}) \triangleq \begin{bmatrix} \Re[V_1(x_1 + iy_1, x_2 + iy_2)] \\ -\Im[V_1(x_1 + iy_1, x_2 + iy_2)] \\ \Re[V_2(x_1 + iy_1, x_2 + iy_2)] \\ -\Im[V_2(x_1 + iy_1, x_2 + iy_2)] \end{bmatrix}, \quad (1)$$

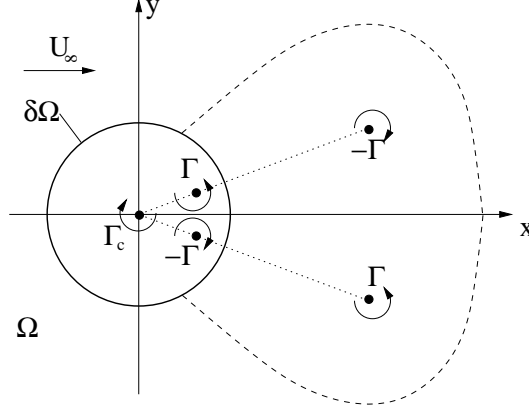


Fig. 2. Schematic of the Föppl point vortex system with actuation represented by the circulation  $\Gamma_c$ . The dashed line represents the boundary of the recirculation region.

where  $\mathbf{X} = [x_1 \ y_1 \ x_2 \ y_2]^T$  and the vortex velocities are given by

$$V_1(z_1, z_2) = 1 - \frac{1}{z_1^2} - \frac{\Gamma}{2\pi i} \left( \frac{1}{z_1 - 1/\bar{z}_2} - \frac{1}{z_1 - 1/\bar{z}_1} - \frac{1}{z_1 - z_2} \right), \quad (2a)$$

$$V_2(z_1, z_2) = 1 - \frac{1}{z_2^2} + \frac{\Gamma}{2\pi i} \left( \frac{1}{z_2 - 1/\bar{z}_1} - \frac{1}{z_2 - z_1} - \frac{1}{z_2 - 1/\bar{z}_2} \right), \quad (2b)$$

where an overbar denotes complex conjugation. The Föppl system is known to possess nonunique equilibrium points [12], i.e., vortex configurations for which  $\frac{d}{dt}\mathbf{X} = 0$ . However, in this investigation we are exclusively interested in one equilibrium, namely corresponding to a flow with a closed recirculation bubble behind the obstacle (Figure 2) in which the singularity location  $(x_0, y_0)$  and its strength  $\Gamma$  are connected through the following relations

$$\begin{cases} (r_0^2 - 1)^2 = 4r_0^2(r_0^2 - x_0^2), \\ \Gamma = 2\pi \frac{(r_0^2 - 1)^2(r_0^2 + 1)}{r_0^5}, \end{cases} \quad (3)$$

where  $x_0 = x_1 = x_2$ ,  $y_0 = y_1 = -y_2$  and  $r_0^2 = x_0^2 + y_0^2$ . We note that relations (3) represent a family of solutions depending on one parameter, for instance, the downstream position  $x_0$  of the vortices. Linear stability of the equilibrium solutions (3) was investigated by several authors including Föppl himself [12], Smith [16], Cai et al. [17], and de Laat and Coene [18]. The study by Tang and Aubry [19] provided a careful analysis of the connection between stability properties of equilibrium (3) and the vortex shedding instability in an actual cylinder wake flow. Non-linear stability of the Föppl system was studied in a weakly nonlinear setting by Tordella in [20] and recently for a more general system using the energy–Casimir methods by Shashikanth et al. in [21]. Local stability is investigated by considering small perturbations  $z'_1 = x'_1 + iy'_1$  and  $z'_2 = x'_2 + iy'_2$  around the equilibrium  $z_0 = x_0 + iy_0$ , i.e.,  $z_1 = z_0 + z'_1$  and  $z_2 = \bar{z}_0 + z'_2$ . Evolution of the perturbation vector

$\mathbf{X}' = [x_1' \ y_1' \ x_2' \ y_2']^T$  is governed by the equation

$$\frac{d}{dt}\mathbf{X}' = \mathbb{A}\mathbf{X}', \quad (4)$$

where  $\mathbb{A} \triangleq \nabla \mathbf{F}(\mathbf{X}_0)$  is the Jacobian of the nonlinear function  $\mathbf{F}(\mathbf{X})$  evaluated at the equilibrium  $\mathbf{X}_0 = [x_0 \ y_0 \ x_0 \ -y_0]^T$ . Thus, the local stability properties are determined by the eigenvalues of the  $4 \times 4$  matrix  $\mathbb{A}$  which turns out to have the following eigenmodes:

- unstable (growing) mode  $\alpha$  corresponding to a positive real eigenvalue  $\lambda_1 = \lambda_r$ ,
- stable (decaying) mode  $\beta$  corresponding to a negative real eigenvalue  $\lambda_2 = -\lambda_r$ ,
- neutrally stable oscillatory mode  $\gamma$  corresponding to a conjugate pair of purely imaginary eigenvalues  $\lambda_3 = -\lambda_4 = i\lambda_i$ ,

where  $\lambda_r, \lambda_i \in \mathbb{R}^+$ . We emphasize that expressions for  $\lambda_r$  and  $\lambda_i$  as well as for the eigenvectors of  $\mathbb{A}$  are available in a closed form which holds regardless of the value of the downstream position  $x_0 > R$  parameterizing the equilibrium solution (3). For further details concerning linear stability of the equilibrium (3) the Reader is referred to [19].

Owing to the presence of the exponentially growing mode  $\alpha$ , the equilibrium solution (3) of system (1) is unstable. In the earlier investigation [15] we considered a stabilization strategy for the Föppl system which used the cylinder rotation, represented by the associated circulation  $\Gamma_C$ , as the flow actuation (Figures 1 and 2). Including the effect of this actuation in system (1) results in the controlled system

$$\frac{d}{dt}\mathbf{X} = \mathbf{F}(\mathbf{X}) + \mathbf{b}(\mathbf{X})\Gamma_C, \quad (5)$$

where the  $4 \times 1$  control matrix is given by

$$\mathbf{b}(\mathbf{X}) = \frac{1}{2\pi} \begin{bmatrix} -y_1/(x_1^2 + y_1^2) \\ x_1/(x_1^2 + y_1^2) \\ y_2/(x_2^2 + y_2^2) \\ x_2/(x_2^2 + y_2^2) \end{bmatrix} \quad (6)$$

and the corresponding linearized controlled system is

$$\frac{d}{dt}\mathbf{X}' = \mathbb{A}\mathbf{X}' + \mathbb{B}\Gamma_C, \quad (7)$$

where  $\mathbb{B} \triangleq \mathbf{b}(\mathbf{X}_0)$ . Controllability of system (7) can be inferred from the rank condition [22]

$$\mathcal{N}_C = \text{rank} [\mathbb{B} \ \mathbb{A}\mathbb{B} \ \mathbb{A}^2\mathbb{B} \ \mathbb{A}^3\mathbb{B}] = 2 \neq \dim(\mathbf{X}) = 4, \quad (8)$$

which indicates that two modes are in fact not controllable. Using transformation to the minimal representation one can identify the uncontrollable part as the mode  $\gamma$  associated with the conjugate pair of purely imaginary eigenvalues  $\pm\lambda_j$ . Thus, owing to the stability of this mode, the linearized system (7) is *stabilizable*, even though it is not *controllable*. Using methods of modern linear control theory [22], a feedback stabilization strategy, known as a Linear–Quadratic–Regulator (LQR), was designed in [15] which rendered the linearized system (7) stable in addition to minimizing a certain performance criterion based on the output of system (7) obtained with a suitably–defined observation operator. In other words, we found a feedback operator  $\mathbb{K} \in \mathbb{R}^{1 \times 4}$  such that the control could be expressed as  $\Gamma_C = -\mathbb{K}\mathbf{X}'$  and the closed–loop system matrix  $(\mathbb{A} - \mathbb{B}\mathbb{K})$  did not have eigenvalues with positive real parts. As a matter of fact, the problem considered in [15] was still somewhat more complicated as a result of certain practical considerations. The stabilization strategy outlined above determines the control based on the instantaneous state  $\mathbf{X}'$  of the perturbation system which in reality is not known. What is, however, available in the considered setting are certain measurements of the system which can be used to construct an evolving estimate of the state using an estimator system such as, for instance, the Kalman filter. Thus, in practice, feedback is determined based on these state estimates, rather than the actual states of the system. Such a combination of a regulator and an estimator is referred to as a compensator. In order to simplify the mathematical analysis, in the present investigation we will however consider an idealized case of feedback control based on the state of the system, rather than its estimate. As illustrated by numerical computations presented in Figures 3a,b, the two cases lead in fact to qualitatively similar results.

The linear stabilization strategy described above was applied in [15], as is often the case, to the original nonlinear Föppl system (5) resulting in

$$\frac{d}{dt}\tilde{\mathbf{X}} = (\mathbb{A} - \mathbb{B}\mathbb{K})\tilde{\mathbf{X}} + \mathbf{G}(\tilde{\mathbf{X}}), \quad (9)$$

where  $\tilde{\mathbf{X}} \triangleq \mathbf{X} - \mathbf{X}_0$  is not assumed small and  $\mathbf{G}(\tilde{\mathbf{X}}) \triangleq \mathbf{F}(\mathbf{X}_0 + \tilde{\mathbf{X}}) - \mathbb{A}\tilde{\mathbf{X}}$  [this change of variables shifts the equilibrium of system (5) to the origin]. The fact that the uncontrollable mode  $\gamma$  is only *neutrally* stable has important consequences, both theoretical and practical, as regards the behavior of the closed–loop nonlinear system (9). As is well known (see, e.g., [23]), when the Jacobian of a nonlinear system calculated at an equilibrium has purely imaginary eigenvalues, it may not be sufficient to determine the local stability of this equilibrium and more information is required for that purpose. The behavior of the closed–loop system with two types of feedback illustrated in Figures 3a,b indicates clearly that after an initial instability is mitigated, in both cases the system trajectory converges to a circular orbit. While it can be anticipated that this observed behavior is a result of the neutral stability of the uncontrollable mode  $\gamma$ , complete characterization of this orbit requires that the full nonlinear system be analyzed, rather than its linearization only. In the next Section we prove that the closed orbit represents in fact a center manifold of system (9) and its persistence is analyzed in Section 4.

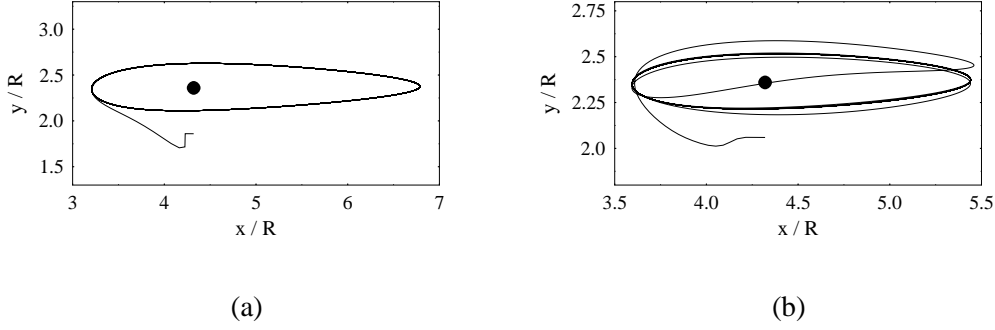


Fig. 3. Trajectories of the upper vortex in (a) closed-loop nonlinear system (9) with state feedback and (b) nonlinear system (5) with feedback determined using estimation-based compensation (see [15]). The solid circles represent the location of the equilibrium (3) corresponding to  $x_0 = 4.32$ .

### 3 Invariant Manifold Reduction of the Controlled Föppl System

We begin this Section by stating the Hamiltonian form of the uncontrolled system (1). This representation will be needed in Section 4 in the proof of the stability of the reduced system. As is well known (see, e.g., [24]), the Hamiltonian is given by

$$\begin{aligned}
 H(x_1, y_1, x_2, y_2) = & \frac{\Gamma^2}{4\pi} \ln |x_1^2 + y_1^2 - 1| + \frac{\Gamma^2}{4\pi} \ln |x_2^2 + y_2^2 - 1| + \frac{\Gamma^2}{2\pi} \ln \sqrt{(x_1 - x_2)^2 + (y_1 - y_2)^2} \\
 & - \frac{\Gamma^2}{2\pi} \ln \sqrt{1 - 2(x_1 x_2 + y_1 y_2) + (x_1^2 + y_1^2)(x_2^2 + y_2^2)} \\
 & - \Gamma \left( y_1 - \frac{y_1}{x_1^2 + y_1^2} \right) + \Gamma \left( y_2 - \frac{y_2}{x_2^2 + y_2^2} \right),
 \end{aligned} \tag{10}$$

so that the equations of motion can be expressed as

$$\left\{ \begin{array}{l}
 (-\Gamma) \dot{x}_1 = \frac{\partial H}{\partial y_1}, \\
 \Gamma \dot{x}_2 = \frac{\partial H}{\partial y_2}, \\
 (-\Gamma) \dot{y}_1 = -\frac{\partial H}{\partial x_1}, \\
 \Gamma \dot{y}_2 = -\frac{\partial H}{\partial x_2}.
 \end{array} \right. \tag{11}$$

We now shift the equilibrium position to the origin using the substitution  $\mathbf{X} = \mathbf{X}_0 + \tilde{\mathbf{X}}$  and introduce the following *symplectic* transformation

$$\Xi = \begin{bmatrix} \eta_1 & \xi_2 & \xi_1 & \eta_2 \end{bmatrix}^T \triangleq \mathbb{Z} \tilde{\mathbf{X}} \tag{12}$$

defined by the matrix

$$\mathbb{Z} \triangleq \frac{1}{\sqrt{2}} \begin{bmatrix} 1 & 0 & -1 & 0 \\ 0 & 1 & 0 & -1 \\ 1 & 0 & 1 & 0 \\ 0 & 1 & 0 & 1 \end{bmatrix}. \quad (13)$$

(the reason for the special ordering of the elements of the vector  $\Xi$  will become apparent below). As a result of these transformations, system (1)–(2) can be rewritten as

$$\begin{cases} \Gamma \dot{\eta}_1 = \frac{\partial \tilde{H}}{\partial \xi_1}, \\ \Gamma \dot{\xi}_2 = \frac{\partial \tilde{H}}{\partial \eta_2}, \\ \Gamma \dot{\xi}_1 = -\frac{\partial \tilde{H}}{\partial \eta_1}, \\ \Gamma \dot{\eta}_2 = -\frac{\partial \tilde{H}}{\partial \xi_2}, \end{cases} \quad (14)$$

where the new Hamiltonian is  $\tilde{H}(\Xi) \triangleq H(\mathbf{X}_0 + \mathbb{Z}^T \Xi)$ . We now remark that by exchanging the rows one and three in the matrix  $\mathbb{Z}$  we in fact recover the transformation

$$\mathbb{T} \triangleq \begin{bmatrix} 0 & 0 & 1 & 0 \\ 0 & 1 & 0 & 0 \\ 1 & 0 & 0 & 0 \\ 0 & 0 & 0 & 1 \end{bmatrix} \mathbb{Z} = \frac{1}{\sqrt{2}} \begin{bmatrix} 1 & 0 & 1 & 0 \\ 0 & 1 & 0 & -1 \\ 1 & 0 & -1 & 0 \\ 0 & 1 & 0 & 1 \end{bmatrix} \quad (15)$$

introduced in [15] in order to convert the perturbation system (7) to the minimal representation in which the controllable and uncontrollable parts are uncoupled. Hence, making this rearrangement in (14) and restoring the feedback control terms we can rewrite system (9) as

$$\frac{d}{dt} \begin{bmatrix} \boldsymbol{\xi} \\ \boldsymbol{\eta} \end{bmatrix} = \begin{bmatrix} \mathbb{A}_0 & 0 \\ 0 & \mathbb{A}_s \end{bmatrix} \begin{bmatrix} \boldsymbol{\xi} \\ \boldsymbol{\eta} \end{bmatrix} + \begin{bmatrix} \mathbf{g}_1(\boldsymbol{\xi}, \boldsymbol{\eta}) \\ \mathbf{g}_2(\boldsymbol{\xi}, \boldsymbol{\eta}) \end{bmatrix}, \quad (16)$$

where  $\boldsymbol{\xi} \triangleq [\xi_1 \ \xi_2]^T$  and  $\boldsymbol{\eta} \triangleq [\eta_1 \ \eta_2]^T$ . The linear and nonlinear parts of system (16) are obtained as

$$\begin{bmatrix} \mathbb{A}_0 & 0 \\ 0 & \mathbb{A}_s \end{bmatrix} = \mathbb{T}(\mathbb{A} - \mathbb{B}\mathbb{K})\mathbb{T}^T, \quad (17)$$

$$\begin{bmatrix} \mathbf{g}_1(\boldsymbol{\xi}, \boldsymbol{\eta}) \\ \mathbf{g}_2(\boldsymbol{\xi}, \boldsymbol{\eta}) \end{bmatrix} = \mathbb{T}\mathbf{G} \left( \mathbb{T}^T \begin{bmatrix} \boldsymbol{\xi} \\ \boldsymbol{\eta} \end{bmatrix} \right). \quad (18)$$

As shown in [15], the first row of (16) represents the uncontrollable part of the linearized system (7) and the matrix  $\mathbb{A}_0$  has a conjugate pair of purely imaginary eigenvalues, whereas the second row of (16) represents the controllable part of system (7) and, due to the effect of the feedback term, the matrix  $\mathbb{A}_s$  has eigenvalues with negative parts only.

Transformation (15) splits the state space  $\mathbb{R}^4$  into two subspaces  $W_c$  and  $W_s$ , i.e.,  $W_c \times W_s = \mathbb{R}^4$ , such that  $\boldsymbol{\xi} \in W_c$  and  $\boldsymbol{\eta} \in W_s$ . We now recall (see, e.g., [25]) that an *invariant* manifold, characterized by a smooth function  $\boldsymbol{\Phi} : W_c \rightarrow W_s$ , is a set  $\mathcal{M} \subset W_c$  such that if  $\boldsymbol{\xi}(0) \in \mathcal{M}$  and  $\boldsymbol{\eta}(0) = \boldsymbol{\Phi}(\boldsymbol{\xi}(0))$ , then  $\boldsymbol{\xi}(t) \in \mathcal{M}$  and  $\boldsymbol{\eta}(t) = \boldsymbol{\Phi}(\boldsymbol{\xi}(t))$  for all times  $t \in \mathbb{R}^+$ . The following Theorem shows that system (16) has an invariant manifold with a particularly simple structure:

**Theorem 1** *System (16) possesses an invariant manifold given by*

$$\boldsymbol{\Phi}(\boldsymbol{\xi}) = \begin{bmatrix} 0 \\ 0 \end{bmatrix}. \quad (19)$$

**PROOF.** We consider the term  $\mathbf{g}_2(\boldsymbol{\xi}, \boldsymbol{\eta})$  in which we set  $\boldsymbol{\eta} = \boldsymbol{\Phi}(\boldsymbol{\xi})$ . Using (19) we conclude by inspection that in fact  $\mathbf{g}_2(\boldsymbol{\xi}, \mathbf{0}) \equiv \mathbf{0}$ , and therefore  $\boldsymbol{\eta}(t) = \mathbf{0}$  if  $\boldsymbol{\eta}(0) = \mathbf{0}$ . (We remark that the actual expression for  $\mathbf{g}_2(\boldsymbol{\xi}, \boldsymbol{\eta})$  is too long to be presented here, however, all the calculations can be reproduced using the MAPLE code mentioned in Section 1).  $\square$

Thus, the invariant manifold coincides with the subspace  $W_c$ . We note that, since the matrix  $\mathbb{A}_0$  has only purely imaginary eigenvalues, the invariant manifold is in fact a *center manifold* (see, e.g., [26]). Given (19), we can now perform an invariant reduction of (16) and the reduced system on the center manifold is given by

$$\dot{\boldsymbol{\xi}}_0 = \mathbb{A}_0 \boldsymbol{\xi}_0 + \mathbf{g}_1(\boldsymbol{\xi}_0, \mathbf{0}). \quad (20)$$

We remark that application of the feedback control represented by the term  $\mathbb{B}\mathbb{K}\tilde{\mathbf{X}}$  in (9), while stabilizing locally this system, may in general break the Hamiltonian structure of the system. However, we recall that  $\mathbb{T}$  represents a transformation to the minimal representation, so that

$$\mathbb{T}\mathbb{B}\mathbb{K}\mathbb{T}^T = \begin{bmatrix} 0 & 0 \\ 0 & \mathbb{B}_0\mathbb{K}_0 \end{bmatrix},$$

where  $\mathbb{B}_0\mathbb{K}_0$  is a  $2 \times 2$  block. This, together with Theorem 1, implies that the reduced system (20) is in fact invariant with respect to the feedback control. This

observation will play an important role in the proof of stability of the reduced system in the next Section.

#### 4 Stability of the Reduced System

In this Section we show that the reduced system (20) on the center manifold has in fact periodic solutions and that its origin is stable. The first part of this result is made precise in the following theorem:

**Theorem 2** *The reduced system (20) has a one-parameter family of closed orbits (periodic solutions) in a open neighborhood of the origin.*

**PROOF.** On the center manifold, i.e., for  $\eta_1 = \eta_2 = 0$ , the feedback control term vanishes, hence the reduced Hamiltonian  $\tilde{H}_0(\xi_1, \xi_2) \triangleq \tilde{H}(0, \xi_2, \xi_1, 0)$  is conserved along trajectories of the reduced system (20) [a complete expression for  $\tilde{H}_0(\xi_1, \xi_2)$  is given in (A.1) in Appendix A]. Hence, trajectories of solutions of (20) coincide with isocontours of  $\tilde{H}_0(\xi_1, \xi_2)$  and existence of periodic orbits follows from ellipticity of  $\tilde{H}_0(\xi_1, \xi_2)$  in the neighborhood of the origin  $(0, 0)$ . This is shown by expanding  $\tilde{H}_0(\xi_1, \xi_2)$  in a Taylor series about the origin and truncating terms of order 3

$$\tilde{H}_0(\xi_1, \xi_2) = \tilde{H}_0(0, 0) + \frac{1}{2} \begin{bmatrix} \xi_1 & \xi_2 \end{bmatrix} \mathbb{S} \begin{bmatrix} \xi_1 \\ \xi_2 \end{bmatrix} + O(\xi_1^{\alpha_1} \xi_2^{\alpha_2}), \quad (21)$$

where  $\alpha_1 + \alpha_2 = 3$  and  $\mathbb{S}$  is the Hessian matrix

$$\mathbb{S} \triangleq \begin{bmatrix} \frac{\partial^2 \tilde{H}_0}{\partial \xi_1^2}(0, 0) & \frac{\partial^2 \tilde{H}_0}{\partial \xi_1 \partial \xi_2}(0, 0) \\ \frac{\partial^2 \tilde{H}_0}{\partial \xi_1 \partial \xi_2}(0, 0) & \frac{\partial^2 \tilde{H}_0}{\partial \xi_2^2}(0, 0) \end{bmatrix}. \quad (22)$$

The quantity  $\tilde{H}_0(\xi_1, \xi_2)$  is elliptic in the neighborhood of the origin, if the eigenvalues  $\lambda_{s_1}$  and  $\lambda_{s_2}$  of its Hessian  $\mathbb{S}$  have the same sign. As indicated by Figure 4, these eigenvalues, given by expressions (A.2) and (A.3) in Appendix A, indeed have the same sign for all values of  $x_0 > R$  parameterizing the equilibrium solution (3) of the Föppl system. Thus, we conclude that the reduced system (20) has closed trajectories in the neighborhood of the origin, which completes the proof.  $\square$

The reduced Hamiltonian  $\tilde{H}_0(\xi_1, \xi_2)$  may thus serve, after some trivial modifications, as the Lyapunov function for system (20) and its invariance along the trajectories implies stability of the origin. We conclude this Section by stating a corollary addressing stability of the complete Föppl system:

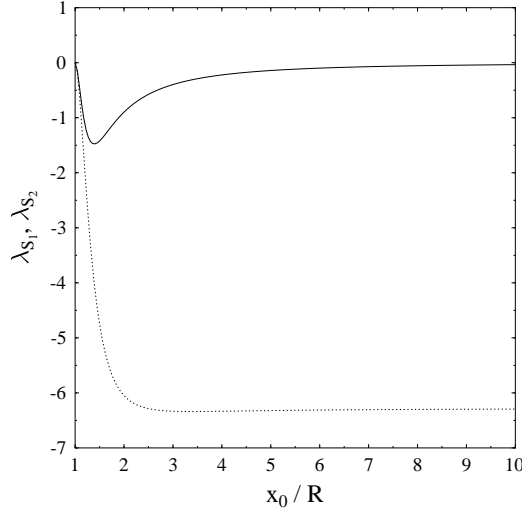


Fig. 4. Eigenvalues  $\lambda_{s_1}$  and  $\lambda_{s_2}$  of the Hessian matrix  $\mathbb{S}$  [Eq. (22)] as a function of the downstream position  $x_0$  of the equilibrium (3).

**Corollary 3** *For initial conditions sufficiently close to equilibrium (3), solutions of the closed-loop Föppl system (9) converge as  $t \rightarrow \infty$  to periodic orbits.*

**PROOF.** This Corollary is a consequence of Theorems 1 and 2, and the local exponential stability of the subsystem  $\dot{\boldsymbol{\eta}} = \mathbb{A}_s \boldsymbol{\eta} + \mathbf{g}_2(\boldsymbol{\xi}, \boldsymbol{\eta})$ .  $\square$

## 5 Computational Results

In this Section we show some numerical results illustrating our findings from Sections 3 and 4. In Fig. 5a we show the error  $\|\boldsymbol{\xi}(t) - \boldsymbol{\xi}_0(t)\|$  between the trajectory of the original system (16) projected on the center manifold  $W_c$  and the trajectory  $\boldsymbol{\xi}_0(t)$  of the reduced system (20) starting from the same initial condition. We note that, as anticipated based on the exponential stability of the subsystem on the stable manifold  $W_s$ , the trajectories converge at an exponential rate. In fact, numerical calculation of the error  $\|\boldsymbol{\xi}(t) - \boldsymbol{\xi}_0(t)\|$  is a rather delicate matter due to accumulation of truncation and round-off errors during integration which eventually obscure any actual error. Despite the use of a high (seventh) order time-integration scheme, this effect is responsible for the increase of the error observed for  $t > 20000$  in Fig. 5a. In Fig. 5b we show the trajectories  $\boldsymbol{\xi}(t)$  and  $\boldsymbol{\eta}(t)$  obtained by solving the original problem (16) which illustrate the behavior of the state projected on the center and

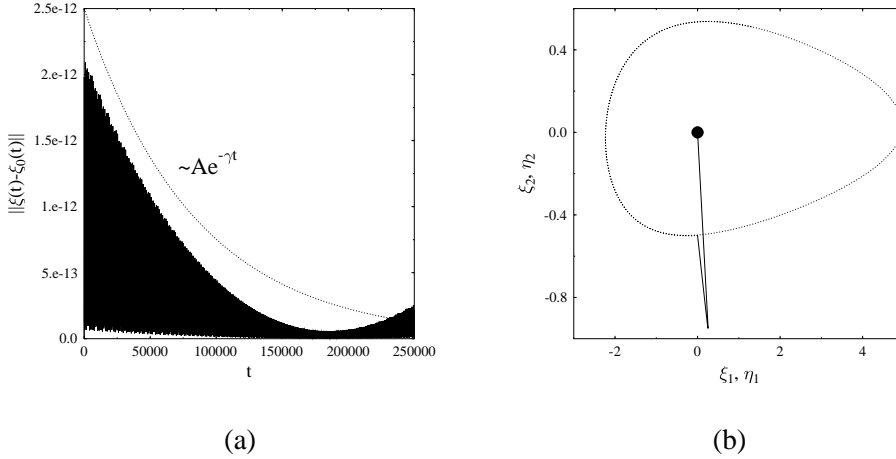


Fig. 5. (a) Time evolution of the error between the trajectory of the original system (16) projected on the center manifold  $W_c$  and the trajectory of the reduced system (20). For comparison the dotted line shows the exponential function  $Ae^{-\gamma t}$ , where  $A, \gamma \in \mathbb{R}^+$ . (b) The time evolution of the (solid line) stable and (dotted line) center manifold parts, respectively  $\eta(t)$  and  $\xi(t)$ , of the original system (16).

stable manifolds,  $W_c$  and  $W_s$ , respectively. We remark that these results confirm predictions of our Corollary 3.

## 6 Conclusions

In this investigation we provided a precise mathematical characterization of the behavior observed as a result of application of a simplified linear feedback control strategy to stabilize the equilibrium of the Föppl point vortex system. The simplification consisted in studying a state–feedback regulator (LQR) instead of an estimator–based feedback compensator (LQG) actually used in the original investigation [15] and was motivated by the need to avoid the analytical complexity of the latter. However, as the results presented in Figure 3 indicate, the behavior in the two cases appears qualitatively similar, hence we believe that the results obtained here can also explain the behavior observed when an actual LQG compensator was applied.

We proved that the uncontrollable subspace of the linearized system (7) coincides in fact with the center manifold of the full closed–loop nonlinear system (9). Thus, the long–time behavior of the controlled system is determined by the properties of the reduced system (20) on the center manifold which was proved to sustain, for bounded initial data, periodic oscillations. Therefore, the oscillations of the controlled system observed in computations reported in [15] have generic character. We remark that analogous behavior was also observed during stabilization of other

vortex-dominated flows (cf. Fig. 21 in [8]).

We emphasize that these nonvanishing oscillations are a rather undesirable property of the Föppl system employed as a reduced-order model for control design, especially when applied afterwards to the full Navier–Stokes system. We believe that this property was in fact responsible for the difficulties that this control strategy experienced in completely stabilizing the near wake region of an actual 2D cylinder wake flow, as also reported in [15]. One possible remedy is to “redesign” the Föppl system, so that the uncontrollable modes will be asymptotically stable. It turns out that this is in fact possible and can be done by constructing a family of “higher-order Föppl systems”, an approach discussed in detail in [27]. Preliminary computational results concerning feedback stabilization of such higher-order Föppl systems are reported in [28]. Another interesting and potentially promising possibility is to investigate the existence of “flat” coordinates in the controlled Föppl system in the spirit of the study [9]. We remark that, due to the properties of the invariant manifold reduction which leaves  $\xi$  and  $\eta$  uncoupled, the coordinates  $\Xi$  are not flat.

## Acknowledgments

It is this author’s pleasure to acknowledge many interesting and stimulating discussions with Dr. Dmitry Pelinovsky, as well as his constructive feedback concerning an earlier version of the manuscript. The research was supported by NSERC–Discovery (Canada) and CNRS (France).

## A Reduced Hamiltonian $\tilde{H}$ and Eigenvalues of its Hessian

The reduced Hamiltonian  $\tilde{H}(\Xi)$  on the center manifold  $W_c$  is given by

$$\begin{aligned}
\tilde{H}_0(\xi_1, \xi_2) = & -\Gamma \left[ y_0 + \frac{\sqrt{2}}{2}\xi_2 - \frac{y_0 + \frac{\sqrt{2}}{2}\xi_2}{\left(x_0 + \frac{\sqrt{2}}{2}\xi_1\right)^2 + \left(y_0 + \frac{\sqrt{2}}{2}\xi_2\right)^2} \right] \\
& + \Gamma \left[ -y_0 - \frac{\sqrt{2}}{2}\xi_2 - \frac{-y_0 - \frac{\sqrt{2}}{2}\xi_2}{\left(x_0 + \frac{\sqrt{2}}{2}\xi_1\right)^2 + \left(-y_0 - \frac{\sqrt{2}}{2}\xi_2\right)^2} \right] \\
& + 2\frac{\Gamma^2}{4\pi} \ln \left[ \left(x_0 + \frac{\sqrt{2}}{2}\xi_1\right)^2 + \left(y_0 + \frac{\sqrt{2}}{2}\xi_2\right)^2 - 1 \right] + \frac{\Gamma^2}{4\pi} \ln \left( 4y_0^2 + 4y_0\sqrt{2}\xi_2 + 2\xi_2^2 \right) \\
& - \frac{\Gamma^2}{4\pi} \ln \left\{ \frac{\sqrt{2}}{4} \left[ 4y_0\xi_2^3 + 4x_0\xi_2^2\xi_1 + 8y_0\xi_2 \left( r_0^2 + \frac{1}{4}\xi_1^2 + 1 \right) + 8x_0\xi_1 \left( r_0^2 + \frac{1}{4}\xi_1^2 - 1 \right) \right] \right. \\
& + \frac{1}{2} \left( 2 + 2x_0^2 + 6y_0^2 + \xi_1^2 \right) \xi_2^2 + 4\xi_1 y_0 \xi_2 x_0 + \frac{1}{4}\xi_1^4 + (3x_0^2 + y_0^2 - 1) \xi_1^2 \\
& \left. + x_0^4 + \frac{1}{4}\xi_2^4 + 2(y_0^2 - 1)x_0^2 + (y_0^2 + 1)^2 \right\}.
\end{aligned} \tag{A.1}$$

The eigenvalues of the Hessian matrix  $\mathbb{S}$  are expressed as

$$\lambda_{s_1} = -\frac{\Gamma}{16} \frac{\Gamma \pi r_0^4 (r_0^2 - 2x_0 + 1)^2 (r_0^2 + 2x_0 + 1)^2 + 16\pi r_0 \sqrt{Q}}{\pi^2 y_0^2 r_0^4 (r_0^2 - 1)^2 (r_0^2 - 2x_0 + 1) (r_0^2 + 2x_0 + 1)}, \tag{A.2}$$

$$\lambda_{s_2} = -\frac{\Gamma}{16} \frac{\Gamma \pi r_0^4 (r_0^2 - 2x_0 + 1)^2 (r_0^2 + 2x_0 + 1)^2 - 16\pi r_0 \sqrt{Q}}{\pi^2 y_0^2 r_0^4 (r_0^2 - 1)^2 (r_0^2 - 2x_0 + 1) (r_0^2 + 2x_0 + 1)}, \tag{A.3}$$

where  $Q$  is given by

$$\begin{aligned}
Q = & \pi^2 \left[ y_0^2 + (1+x_0)^2 \right]^2 \left[ y_0^2 + (x_0-1)^2 \right]^2 y_0^4 (r_0^2 - 1)^4 \\
& - \frac{\Gamma\pi}{8} y_0^3 (r_0^2 - 1)^2 \left[ y_0^{14} + (3x_0^2 + 22)y_0^{12} + (-3x_0^4 + 96x_0^2 + 31)y_0^{10} \right. \\
& + (4 - 25x_0^6 + 182x_0^4 + 47x_0^2)y_0^8 + (-45x_0^8 - 72x_0^2 - 26x_0^4 - 1 + 208x_0^6)y_0^6 \\
& + (-96x_0^4 - 114x_0^6 + 6 + 162x_0^8 + 81x_0^2 - 39x_0^{10})y_0^4 + \\
& \left. (80x_0^{10} + 1 - 17x_0^{12} - 117x_0^8 + 40x_0^6 - 24x_0^2 + 37x_0^4)y_0^2 - 3x_0^2 (x_0 - 1)^6 (1 + x_0)^6 \right] \\
& + \frac{\Gamma^2 r_0^6}{256} \left[ y_0^{16} + (8x_0^2 + 40)y_0^{14} + (380 + 8x_0^2 + 28x_0^4)y_0^{12} \right. \\
& + (56x_0^6 + 1480x_0^2 - 376x_0^4 - 392)y_0^{10} + (70x_0^8 + 2404x_0^4 - 1688x_0^2 + 262 - 792x_0^6)y_0^8 \\
& + (856x_0^2 - 648x_0^8 + 56x_0^{10} - 40 - 2128x_0^4 + 1904x_0^6)y_0^6 \\
& + 28(1+x_0)^4 \left( x_0^4 - \frac{30}{7}x_0^2 - \frac{1}{7} \right) (x_0 - 1)^4 y_0^4 + 8(x_0^2 + 1)(x_0 - 1)^6 (1+x_0)^6 y_0^2 \\
& \left. + (x_0 - 1)^8 (1+x_0)^8 \right].
\end{aligned}$$

## References

- [1] T. R. Bewley, "Flow control: new challenges for a new Renaissance", *Progress in Aerospace Sciences* **37**, 21-58, (2001).
- [2] J. Kim, "Control of turbulent boundary layers", *Phys. Fluids* **15**, 1093-1105, (2003).
- [3] L. Cortelezzi, A. Leonard and J. C. Doyle, "An example of active circulation control of the unsteady separated flow past a semi-infinite plate", *J. Fluid Mech.* **260**, 127-154, (1994).
- [4] L. Cortelezzi, "Nonlinear feedback control of the wake past a plate with a suction point on the downstream wall", *J. Fluid Mech.* **327**, 303-324, (1996).
- [5] L. Cortelezzi, Y. -C. Chen and H. -L. Chang, "Nonlinear feedback control of the wake past a plate: from a low order model to a higher order model", *Phys. Fluids* **9** (7), 2009-2022, (1997).
- [6] S. I. Chernyshenko, "Stabilization of trapped vortices by alternating blowing and suction", *Phys. Fluids* **7** (4), 802-801, (1995).
- [7] Á. Péntek, J. B. Kadtko and G. Pedrizzetti, "Dynamical control for capturing vortices near bluff bodies", *Phys. Rev. E*, **58** (2), 1883-1898, (1998).
- [8] L. Zannetti and A. Iollo, "Passive control of the vortex wake past a flat plate at incidence", *Theoretical and Computational Fluid Dynamics* **16**, 211-230, (2003).

- [9] B. R. Noack, A. Banaszuk and I. Mezić, “Controlling vortex motion and chaotic advection”, *Proceedings of the 39th IEEE Conference on Decision and Control*, paper INV 4902, (2000).
- [10] B. R. Noack, I. Mezić, G. Tadmor and A. Banaszuk, “Optimal mixing in recirculation zones”, *Phys. Fluids* **16** (4), 867-888, (2004).
- [11] D. L. Vainchtein and I. Mezić, “Optimal control of a co-rotating vortex pair: averaging and impulsive control”, *Physica D* **192**, 63-82, (2004).
- [12] L. Föppl, “Wirbelbewegung hinter einem Kreiscylinder”, *Sitzb. d. k. Bayer. Akad. d. Wiss.* **1**, 1-17, (1913).
- [13] S. Tang and N. Aubry, “Suppression of vortex shedding inspired by a low-dimensional model”, *J. Fluids and Struct.* **14**, 443-468, (2000).
- [14] F. Li and N. Aubry, “Feedback control of a flow past a cylinder via transverse motion”, *Physics of Fluids* **15**, 2163-2176, (2003).
- [15] B. Protas, “Linear Feedback Stabilization of Laminar Vortex Shedding Based on a Point Vortex Model”, *Physics of Fluids* **16**(12), 4473-4488, 2004.
- [16] A. C. Smith, “On the stability of Föppl vortices”, *J. Appl. Mech* **70**, 610, (1973).
- [17] J. Cai, F. Liu and S. Luo, “Stability of a Vortex Pair behind Two-Dimensional Bodies”, *AIAA Paper* 2001-2844, (2001).
- [18] T. W. G. de Laat and R. Coene, “Two-dimensional vortex motion in the cross-flow of a wing-body configuration”, *J. Fluid Mech.* **305**, 93-109, (1995).
- [19] S. Tang and N. Aubry, “On the symmetry breaking instability leading to vortex shedding”, *Physics of Fluids* **9**, 2550-2561, (1997).
- [20] D. Tordella, “Nonsteady stability of the flow around the circle in the Föppl model”, *Quart. Appl. Math.* **53**, 683, (1995).
- [21] B. N. Shashikanth, J. E. Marsden, J. W. Burdick and S. D. Kelly, “The Hamiltonian structure of a two-dimensional rigid circular cylinder interacting dynamically with  $N$  point vortices”, *Physics of Fluids* **14**, 1214, (2002).
- [22] R. F. Stengel, “Optimal Control and Estimation”, Dover Publications, (1994).
- [23] H. K. Khalil, “Nonlinear Systems”, Prentice-Hall, (2002).
- [24] H. H. Luihardt, J.B. Kadtke and G. Pedrizzetti, “Chaotic capture of vortices by a moving body II. Bound pair model”, *Chaos* **4**, 681, (1994)
- [25] S. Wiggins, “Introduction to Applied Nonlinear Dynamical Systems and Chaos”, Springer, (1990).
- [26] J. Carr, “Applications of Centre Manifold Theory”, Springer, (1981).
- [27] B. Protas, “Higher-order Föppl models of steady wake flows”, *Physics of Fluids* **18** (11), 117109, 2006.

- [28] B. Protas, “Vortex models for feedback stabilization of wake flows”, In R. King (Ed.) *Active Flow Control (Papers contributed to the Conference “Active Flow Control 2006”, Berlin, Germany, September 27–29, 2006)*, Notes on Numerical Fluid Mechanics and Multidisciplinary Design, Springer (in press), 2007.